Studies of dE/dx measurements with the BESIII *

CAO Xue-Xiang(曹学香)[1,2;1)] LI Wei-Dong(李卫东)[1;2)] Roy A. Briere[3] LIU Chun-Lei(刘春雷)[3]
MAO Ze-Pu(毛泽普)[1] CHEN Shen-Jian(陈申见)[4] DENG Zi-Yan(邓子艳)[1] HE Kang-Lin(何康林)[1]
HUANG Xing-Tao(黄性涛)[5] HUANG Bin(黄彬)[1] HUANG Yan-Ping(黄艳萍)[1,2] JIA Lu-Kui(贾卢魁)[1,2]
JI Xiao-Bin(季晓斌)[1] LI Xiu-Rong(李秀荣)[1,2] LIU Chun-Yan(刘春燕)[1,2] LIU Huai-Min(刘怀民)[1]
MA Qiu-Mei(马秋梅)[1] MA Xiang(马想)[1] QIU Jin-Fa(邱进发)[1] WANG Da-Yong(王大勇)[1]
WU Ling-Hui(伍灵慧)[1] WU Zhi(吴智)[1,2] YUAN Ye(袁野)[1] ZHANG Xue-Yao(张学尧)[5]
ZHAO Chuan(赵川)[6] ZHANG Yao(张瑶)[1] ZOU Jia-Heng(邹佳恒)[1]

[1] Institute of High Energy Physics, CAS, Beijing 100049, China
[2] Graduate University of Chinese Academy of Sciences, Beijing 100049, China
[3] Carnegie Mellon University, Pittsburgh, PA 15213, USA
[4] Nanjing University, Nanjing 210093, China
[5] Shandong University, Jinan 250100, China
[6] Department of Modern Physics, University of Science and Technology of China, Hefei 230026, China

Abstract The Beijing Spectrometer III (BESIII) is a general-purpose detector used for the study of τ-charm physics at the Beijing Electron-Positron Collider II (BEPC II). This paper presents our studies of the dE/dx measurement in the drift chamber of BESIII, which is important for the identification of charged particles. Corrections applied to the dE/dx measurement in data reconstruction are discussed. After our current dE/dx calibration, a resolution of about 6% has been obtained for minimum ionization particles, and a 3σ K/π separation is obtained for momenta up to 760 MeV/c. These results meet the design goals of the BESIII drift chamber.

Key words BESIII drift chamber, energy loss, dE/dx, calibration, particle identification

PACS 29.40.Cs, 34.50.Bw

1 Introduction

The Beijing Spectrometer III (BESIII) [1] is a general-purpose detector working at the upgraded Beijing Electron-Positron Collider II (BEPC II). It is designed for detecting the various final states produced in e^+e^- collisions near center-of-mass energies of about 3–4 GeV. Physics research goals include charmonium physics, D-physics, spectroscopy of light hadrons and τ-physics, as well as searches for new physical interactions and phenomena. The rich physics program of BESIII not only requires high-precision momentum measurements of charged particles but also necessitates good particle identification.

The BESIII detector [2] is composed of the following four main sub-detectors: the Main Drift Chamber (MDC), the Time Of Flight (TOF), the Electric-Magnetic Calorimeter (EMC) and the Muon Chamber (MUC). The MDC sub-detector determines the momentum, direction and vertex position for charged particles [3]. It can also be used for particle identification via the specific energy loss, dE/dx, of charged particles traversing the MDC. Momentum resolution is improved by choosing materials to reduce multiple scattering. For this purpose, a helium-based gas mixture (60/40 He/C_3H_8) [4] is chosen as the working gas of the MDC; this choice will also lead to a good dE/dx resolution. As shown in Fig. 1, the drift cha-

Received 3 March 2010, Revised 12 April 2010

* Supported by National Natural Science Foundation of China (10821063, 10875141, 10705034, 10605030), Ministry of Science and Technology of China (2009CB825200), Chinese Academy of Sciences (CAS) Large-Scale Scientific Facility Program (KJCX2-YW-N29, KJCX2-YW-N45) and United States Department of Energy (DE-FG02-91ER40682)

1) E-mail: xcao@mail.ihep.ac.cn

2) E-mail: liwd@mail.ihep.ac.cn

mber is divided into two parts, an inner section and an outer section. There are 8 layers in the inner section with an average cell size of about 12 mm×12 mm, and 35 layers in the outer section with a large cell size of about 16.2 mm×16.2 mm. The MDC covers a polar-angle range of $-0.93 \leqslant \cos\theta \leqslant 0.93$, and it has maximum length of 2308 mm. The MDC employs an approximately square drift cell, with each sense wire surrounded by eight field wires, shared with neighboring cells. Sense wires are also staggered in adjacent layers to resolve the left-right ambiguity inherent in drift-distance measurements.

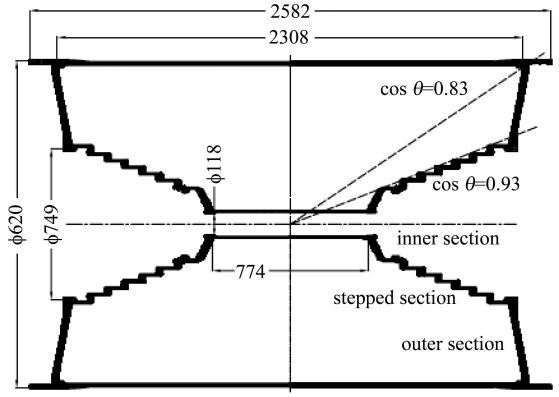

Fig. 1. r-z view of the MDC.

This paper focuses on the dE/dx measurement in the MDC. The ionization is a function of the particle velocity and can hence be used for the identification of different species of charged particles. Section 2 discusses the physics of ionization, Section 3 introduces the various types of corrections applied to dE/dx measurement, and Section 4 gives a detailed description of the dE/dx reconstruction procedure. Section 5 summarizes the achieved performance of dE/dx measurements at BESIII, based on recent experimental data.

2 Energy loss by charged particles

In a magnetic spectrometer, charged particle momenta can be measured through the curvature of a track in an applied magnetic field. The relation between momentum p and velocity v is [5]

$$v = c^2 p/E = c^2 p/\sqrt{p^2c^2 + m^2c^4}\ , \qquad (1)$$

where c is the velocity of light and m is the particle mass. A measurement of the velocity v, combined with the momentum p, allows the possibility of determining the particle mass and obtaining definitive separation among particle species.

Particles traversing through a gas detector will lose energy primarily by ionization. The most probable energy loss can be described by the Bethe-Bloch formula [6]

$$\left\langle \frac{\mathrm{d}E}{\mathrm{d}x} \right\rangle = D\frac{z^2}{m_\mathrm{e}\beta^2}\left[\ln\frac{2m_\mathrm{e}\mu^2 W_{\max}(\mu)}{I^2} - 2\beta^2 - \delta(\mu)\right], \qquad (2)$$

where $D \equiv 2\pi n_\mathrm{e} e^4/c^2$, $\mu \equiv p/m = \beta\gamma$, n_e and I represent the electron density and mean ionization potential in the gas medium, respectively, z is the atomic number, e and m_e are the electron charge and mass, $W_{\max}(\mu)$ is the maximum energy transferred to the electron in a single collision, β is the ratio of the particle velocity over the velocity of light in the vacuum, $\gamma = 1/\sqrt{1-\beta^2}$, and δ is related to the so-called density effect correction. It is seen that the value of dE/dx thus depends on the velocity of the charged particle, as required to provide the possibility of particle identification.

In a practical experiment, the deposited energy detected by the detector is not the same as the energy loss when the particle passes the detector due to various effects. In practice, the experimental energy loss is a semi-empirical equation. Based on the experience from other experiments [7–13], and our own studies with both Monte Carlo and real experimental data on the BESIII, finally we choose the following equation for most-probable energy loss [14]

$$\left\langle \frac{\mathrm{d}E}{\mathrm{d}x} \right\rangle = \frac{p_1}{\beta^{p_4}}\left\{p_2 - \beta^{p_4} - \ln\left[p_3 + \left(\frac{1}{\beta\gamma}\right)^{p_5}\right]\right\}, \qquad (3)$$

where p_i are the five fitting parameters that can be obtained from data samples. It can be seen that our empirical $\left\langle \frac{\mathrm{d}E}{\mathrm{d}x} \right\rangle$ is similar in form to the Bethe-Bloch result. Our function adequately parameterizes the different regions: a $1/\beta^2$ fall-off at low β, a minimum-ionizing region, and finally a relativistic rise ending in the Fermi plateau (a constant limiting value at very large β). Re-writing in terms of $y \equiv p/m \equiv \beta\gamma$, we obtain

$$\frac{\mathrm{d}E}{\mathrm{d}x}(y) = \frac{p_1(\sqrt{y^2+1})^{p_4}}{y^{p_4}}\left\{p_2 - \ln\left[p_3 + \left(\frac{1}{y}\right)^{p_5}\right]\right\} - p_1. \qquad (4)$$

Our dE/dx measurement is only related to $\beta\gamma = p/m$, and can be combined with a particle's momentum to, in principle, achieve particle identification.

3 dE/dx calibration

A precise and accurate dE/dx measurement is crucial for quality particle identification. But dur-

ing data taking, variations in temperature, atmospheric pressure and other environmental conditions will affect the $\mathrm{d}E/\mathrm{d}x$ measurements. Furthermore, the geometric structure of the MDC and the charge-particle trajectory, and non-uniformity of the electric and magnetic fields, also cause biases in the $\mathrm{d}E/\mathrm{d}x$ measurement. In order to get unbiased $\mathrm{d}E/\mathrm{d}x$ values, a dedicated calibration procedure is critical to achieve the high accuracy required for particle identification.

In our $\mathrm{d}E/\mathrm{d}x$ calibration, the following effects have been considered:

(1) path lengths in each drift cell differ due to variations in the polar angle of the tracks;

(2) path length also varies due to the detailed manner in which each track crosses the projected (approximately) square drift cell;

(3) external atmospheric pressure variations, which directly influence gas density and thus the gas gain;

(4) non-uniformity of gas gain in different MDC cells;

(5) non-uniformity of charge collection across a drift cell, which couples to the detailed track geometry;

(6) a space-charge effect, dependent on the polar angle, which causes a screening of the electric field and leads to gain variations;

(7) predication calibration, including both a determination of the empirical ionization as a function of the particle velocity ($\beta\gamma$) and the $\mathrm{d}E/\mathrm{d}x$ measurement resolution, parameterized as a function of relevant parameters.

The above corrections may be grouped into two categories—hit-level corrections and track-level corrections—according to whether they are applied to the individual ionizations measured from each drift cell, or to the track-average ionization. The hit-level corrections normalize the response of the individual wires in the MDC and also account for the track geometry relative to the drift cell. Track-level corrections are used to treat the space-charge effect.

3.1 $\mathrm{d}E/\mathrm{d}x$ distribution

We first need to have a clear picture of the distribution of measured ionizations in a single drift cell. Fig. 2 shows the distribution of the independent $\mathrm{d}E/\mathrm{d}x$ measurements in a single wire obtained from Bhabha events. These high-energy electrons are at very large $\beta\gamma$ and thus all have the same intrinsic ionization. The distribution is similar to the familiar asymmetric Landau distribution, but a Landau function does not describe the distribution well due to the atomic structure of the material [15]. Many functions have been tried to achieve a better fit result, such as a bifurcated Gaussian, Vavilov function and improved Landau (Mylan) function. Testing with the BESIII experimental data, we find that the Mylan function, $\left(f(x)=p_0\mathrm{e}^{-\frac{1}{2}(\lambda+\mathrm{e}^{-\lambda})}, \text{ where } \lambda=\dfrac{x-p_2}{p_1}\right)$ gives a good description of our $\mathrm{d}E/\mathrm{d}x$ distribution. Table 1 shows the χ^2/ndof of each fitting function, and a fit of Mylan is displayed in Fig. 2.

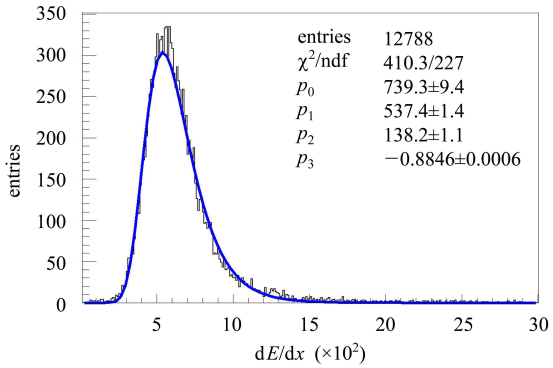

Fig. 2. The distribution of $\mathrm{d}E/\mathrm{d}x$ for a single drift cell (arbitrary units) for Bhabha events. The fitted curve is the Mylan function described in the text.

Table 1. Fitting status.

function	χ^2/ndof
Mylan function	410/227
Bifurcated Gaussian	505/227
Vavilov function	1185/227
Landau	504/228

3.2 $\mathrm{d}E/\mathrm{d}x$ hit-level calibration

3.2.1 Path length correction

Ionization energy loss, $\mathrm{d}E/\mathrm{d}x$, is the energy loss normalized per unit path length. A track that goes near the wire in the cell center creates more ions than a track that goes through the corner. Both this path length in the r-ϕ plane and the path length in the r-z projection affect the measured energy loss. In the procedure of calibration, the r-ϕ path length is first calculated using track parameters and the MDC geometry information. The three-dimensional path length is obtained by dividing this by $\sin\theta$. Then this path is used to normalize our measurements.

3.2.2 Run gain

Gas gain in the detector is affected by environmental changes, most notably the atmospheric pressure[16], and this effect can be absorbed in run

gain correction. Circles on Fig. 3 shows the normalized dE/dx values from Bhabha events. The values change with data run numbers, which crudely translate into time. This figure covers the entire BESIII $\psi(2s)$ data sample from an approximately two-month run in 2009. Fig. 3 shows the variations that are much larger than our final resolution, necessitating a careful correction. We use this Bhabha sample to obtain this gain correction, reflecting the changing environmental situation. After the run gain correction, an overall stability of dE/dx in different runs is obtained, as shown with stars in Fig. 3.

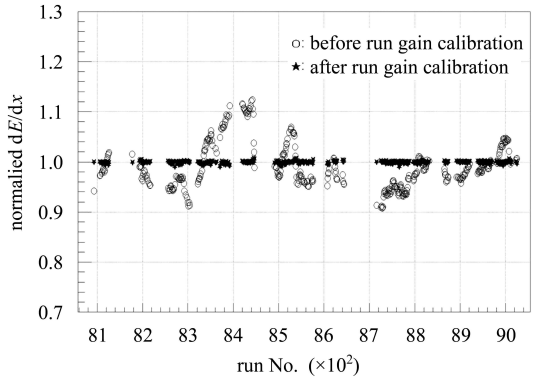

Fig. 3. The normalized dE/dx value versus run number.

3.2.3 Wire gain

The cell geometry and sense wire diameter will affect the gas gain, leading to different gains in different cells. Therefore, a wire gain calibration is performed. Fig. 4 shows the mean dE/dx value versus the wire number. In the figure, the circles show the distribution before calibration; we can clearly see the non-uniformity of dE/dx in different cells. There are four dead wires (Number 1248, 1519, 1534 and 6257) in the MDC, and high voltage is lower in Layer 1 than in Layer 4 (corresponding wires 1 through 188). So

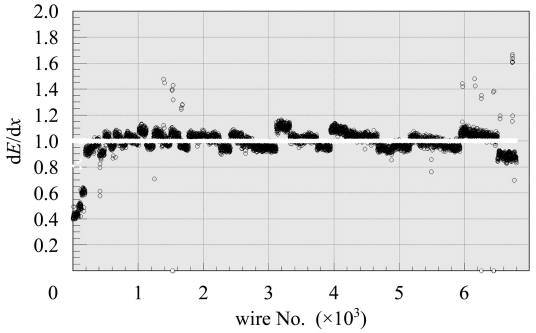

Fig. 4. Results of our wire gain calibration: circles (stars) are the mean values of dE/dx for each drift cell before (after) the wire gain calibration.

those dE/dx values have an even larger deviation from the mean. After the wire gain calibration, a very uniform response is obtained across different cells, as shown with the stars in Fig. 4.

3.2.4 Doca and entrance angle correction

Even after correcting for path length, there are residual effects related to the geometry of the track relative to the sense wire in the r-ϕ projection. This is due to the non-uniformity of charge collection, and the fact that the signal generated by the same ionization in different positions inside a cell could have different amplitudes.

The geometry of the track is described by two variables: the "doca" (the closest approach of the track to the wire) and the "entrance angle" (the angle between the track and the radial direction). We determine an empirical correction using radiative Bhabha events. These electrons all have the same intrinsic ionization, and the range of momenta is needed to cover all possible track geometries.

This empirical 2-D correction plays an important role in removing the asymmetry between positive and negative charged tracks (which differ in the sign of their entrance angle). Fig. 5 shows the improvement of mean value of dE/dx of radiative Bhabha events before and after this correction. The discrepancy between electron and positron becomes much smaller after the correction, and the resolution is also improved.

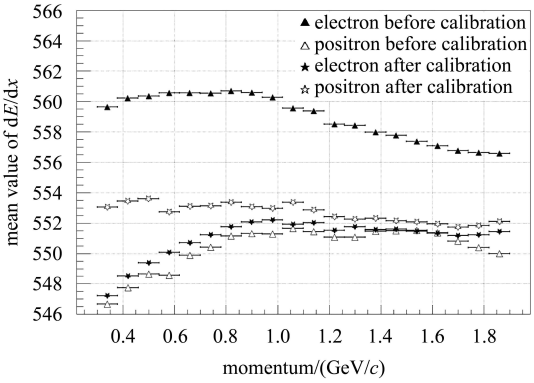

Fig. 5. The distribution of the dE/dx mean value for radiative Bhabha events before and after our empirical track-cell geometry correction.

These hit-level calibrations greatly improve the dE/dx resolution. Before the hit-level calibrations, the dE/dx resolution for Bhabha events is about 6.2%. After the hit-level calibration (and including the electron saturation correction discussed next), the resolution is improved to 4.9%.

3.3 dE/dx track-level calibration

3.3.1 Space charge effect correction

When primary electrons reach a sense wire, they cause an avalanche due to the large electric field: the energy gained in one mean-free path becomes sufficient to ionize further the gas molecules, leading to an avalanche of ionization. This multiplication of the primary electron occurs only very close to the wire, and it acts as a sort of pre-amplifier, with a certain "gas gain". However, the cloud of electrons from one avalanche will reduce the local electric field [17], reducing the gas gain of primary electrons that arrive later. The practical consequence is a dependence of dE/dx on cosθ due to this effect: as the polar angle varies, the charge cloud is spread over different lengths of sense wire in the z direction, leading to variations in the efficiency of the screening. Thus, a space-charge calibration should be applied [11]. The difficulty of doing this calibration is that there is no simple relation of the cosθ dependence at different momentums for different particles, since the intrinsic dE/dx, and hence the amount of screening, varies with momentum as well. For example, the space-charge effect in the $1/\beta^2$ region of large ionization is much larger than in the minimum-ionizing region. We thus need to calibrate as a function of both polar angle and intrinsic ionization: control samples of particles with varying $\beta\gamma$ are needed. In practice, this means we must use many particle types, such as e, μ, π, K, p, over a range of momentum. We first correct for the polar-angle dependence seen in our electron samples, since this can be easily obtained. We then use the other particle samples to do a further calibration, relative to electrons, which takes into account the dependence on intrinsic ionization.

3.3.2 t_0 correction

For charge measurement, a numerical integral method was chosen in the MDC charge readout electronics, based on FADC [2] technology. The basic principle is to successively digitize the input signal with the FADC, and then integrate this digitized data. If the integral window is not wide enough, the full charge will not be measured, and the dE/dx will be smaller than the true ionization. This is not a problem as long as the loss is a constant fraction. However, during our 2009 ψ(2s) data taking, we found that the integration time window was not large enough, and variations in the "t_0" (event start time) [18] led to a variation in the amount of charge loss due to being outside our integration window. Fig. 6(a) shows the relation between t_0 and dE/dx for Bhabha events. It is seen that the dE/dx value decreases as t_0 increases. We obtain a correction from Bhabha events based on the value of dE/dx versus t_0 as seen in this data, and apply this correction to the affected ψ(2s) data sample. Fig. 6(b) shows the performance of the calibration, monitored with pions from the decay $\psi(2s)\to\gamma\chi_c\to\gamma\pi^+\pi^-\pi^+\pi^-$. Due to the difference in trigger conditions, for pions, there are more smaller t_0, most of which come from neutral events trigger in EMC.

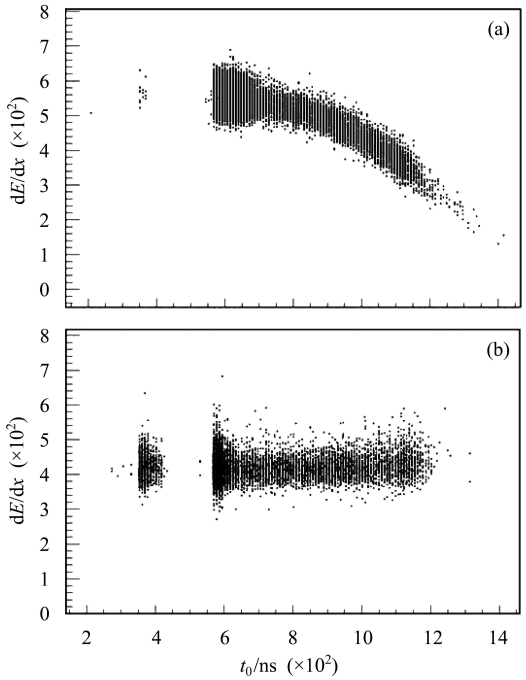

Fig. 6. Scatter plots of dE/dx vs event start time, t_0. Panel (a) shows uncorrected Bhabha electrons, which are used to determine a correction. Panel (b) shows the success of the correction when applied to a sample of pions from $\psi(2s)\to\gamma\chi_c\to\gamma\pi^+\pi^-\pi^+\pi^-$.

3.3.3 Prediction calibration

After various types of hit-level calibrations and track-level corrections are applied to the dE/dx measurement, the truncated mean method (Section 4) is used to calculate the dE/dx value for each track using the energy deposited in the MDC cells. As described in Section 2, the mean value of dE/dx can be parameterized as a function of $\beta\gamma$. Fig. 7 is the dE/dx energy loss curve obtained from $\psi(2s)$ samples, which include five types of particles: e, μ, π, K and p. The following physical channels are chosen for pure control samples because no dE/dx information is needed for event selection:

1) electrons: Bhabha and radiative Bhabha events;

2) muons: cosmic ray events and $e^+e^-\to\mu^+\mu^-$;

3) pions: $\psi(2s)\to\gamma\chi_c\to\gamma\pi^+\pi^-\pi^+\pi^-$;

4) kaons: $\psi(2s)\to\gamma\chi_c\to\gamma K^+K^-K^+K^-$;

5) protons: selected from inclusive $\psi(2s)$ decays using TOF information.

In order to use dE/dx for particle identification, we also need to predict the resolution for any given measurement. With the above control samples, the mean error $\sigma_{\mathrm{d}E/\mathrm{d}x}$ can be parameterized as a function of the mean dE/dx value itself, the track's polar angle, the number of hits available for the track [7, 8], and the event start time (t_0).

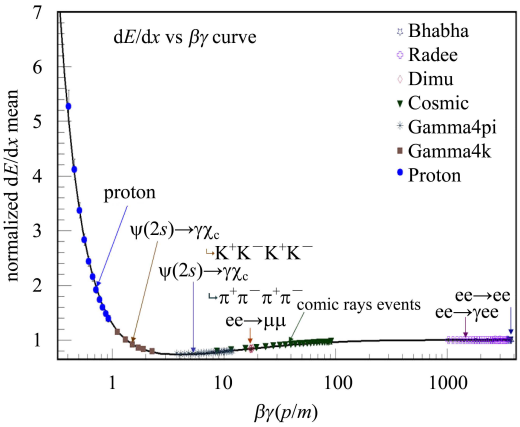

Fig. 7. The energy loss curve fitting with control samples.

4 dE/dx reconstruction

The BESIII offline data reconstruction processes the raw data recorded by the online DAQ system and produces the reconstructed data containing all the information needed by the physics analysis. The dE/dx reconstruction is an important part of this data reconstruction chain. A schematic view of the procedure is shown in Fig. 8. At the calibration stage, the dE/dx calibration algorithm, DedxCalibAlg, produces the calibration constants for all the corrections described in Section 3. Then, the calibration constants are written into the ROOT files and stored in the database, which can be retrieved via the DedxCorrecSvc service at the reconstruction stage. The dE/dx reconstruction mainly consists of the following steps:

①Obtaining the track information from reconstructed track parameters (momentum, polar angle) as well as individual hit information (doca, entrance angle), and so on.

②Applying the basic corrections to get unbiased dE/dx values for hits lying on the track according to the MDC geometry. The basic correction items have been described in Section 3.2; they include the effects of path length, run gain, wire gain and an empirical doca vs. entrance angle correction.

③Using the truncated mean method to get the mean dE/dx value for each track. More details will be given below.

④Applying track-level calibration to remove the space-charge effect described in Section 3.3.

⑤Calculating the normalized deviations of the dE/dx measurement from expectations ("χ") for the e, μ, π, K, p particle hypotheses.

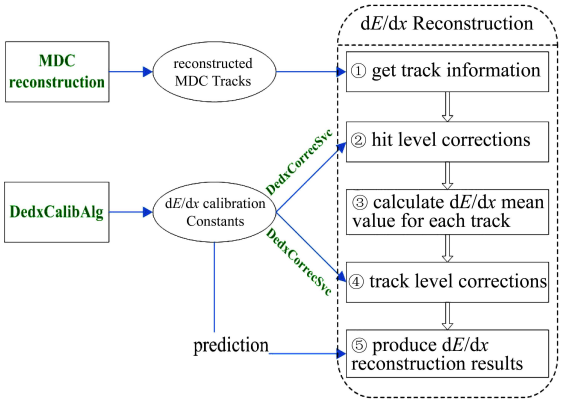

Fig. 8. A chematic view of dE/dx reconstruction flow.

For a given track, every hit on the track offers an energy loss measurement. Energy loss follows a typical Landau distribution due to the statistical fluctuation of gas ionization. A long tail is mainly caused by hard collisions or delta electrons with large energy transfer. In order to get the best unbiased dE/dx value, step ③ is taken after sample measurement of the track in the MDC. Many different methods have been investigated for dE/dx reconstruction: the truncated mean, the double truncated mean, the median, the geometric mean and so on. Considering our needs and the experience of other experiments, the double truncated mean method is adopted here. In this method, both some of the largest values and some of the smallest ones are dropped from the track average, according to a simple prescription, and the rest are used to calculate an average dE/dx value. Based on the studies with MC and real data, we find the best resolution when we keep the 70% of hits that remain after dropping the largest 25% and the lowest 5% of the individual hit measurements. In addition, this truncation method results in a nearly Gaussian resolution function.

After unbiased dE/dx measurement is obtained, step ⑤ produces the normalized dE/dx defined as

$\chi_{\mathrm{d}E/\mathrm{d}x}$

$$\chi_{\mathrm{d}E/\mathrm{d}x}=\frac{\mathrm{d}E/\mathrm{d}x(\mathrm{meas})-\mathrm{d}E/\mathrm{d}x(\mathrm{expect})}{\sigma_{\mathrm{d}E/\mathrm{d}x}}. \quad (5)$$

The $\chi_{\mathrm{d}E/\mathrm{d}x}$ for different particle hypotheses is supplied to users for use in particle-identification algorithms.

5 Performance of dE/dx measurement

The key parameter for evaluating our calibration of the dE/dx measurements is the resolution. With 100 million $\psi(2s)$ events taken in 2009, we have completed the dE/dx calibration and reconstruction. All calibration items mentioned above are taken into account and the double-truncation at 70% is used. A dE/dx resolution of 6% is obtained for minimum-ionizing particles (0.5–0.6 GeV/c π, $\beta\gamma$: 3.6–4.3) for tracks with more than 20 dE/dx samples. This is better than the design goal of the BESIII drift chamber (6%–7%). Fig. 9(a) shows the distribution of minimum-ionizing particles with a Gaussian fit.

Another important parameter to quantify dE/dx measurement is the separation power, which is critical to physics analysis. It reflects the ability of particle identification using the dE/dx measurement. The particle separation power between two types of particle A and B is defined as [13]

$$S_{\mathrm{AB}}=\frac{\Delta E_{\mathrm{AB}}}{\sigma_{\mathrm{AB}}}=\frac{\mathrm{d}E/\mathrm{d}x_{\mathrm{A}}-\mathrm{d}E/\mathrm{d}x_{\mathrm{B}}}{\sigma_{\mathrm{d}E/\mathrm{d}x(\mathrm{AB})}}, \quad (6)$$

where $\sigma_{\mathrm{d}E/\mathrm{d}x(\mathrm{AB})}$ is the average resolution for the two particle species A and B. Fig. 9(b) shows the separation power between two particles as a function of the momentum. The separation power is calculated using the curve in Fig. 7 with $\sigma_{\mathrm{d}E/\mathrm{d}x(\mathrm{AB})}$ from the parameterized function mentioned in Section 3.3.3. Separation power in the low-momentum region (<1 GeV/c), particularly K-π separation, is most important for the BESIII experiment. Currently, 3σ π/K separation can be achieved up to 760 MeV/c, as shown in Fig. 9(b).

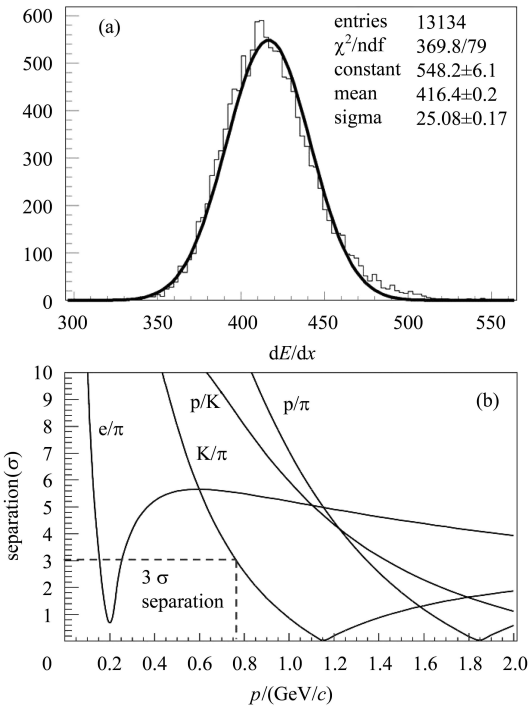

Fig. 9. Performance of dE/dx reconstruction and particle identification ability: (a) resolution for minimum ionization particles (π with momentum of 0.5–0.6 GeV/c, $\beta\gamma$: 3.6–4.3); (b) separation power as a function of momentum.

6 Conclusion

BESIII is a new detector operating at the e^+e^- collider BEPC II. With its first data sample collected at the $\psi(2s)$ peak in 2009, we have completed the dE/dx calibration at both hit-level and track-level. After calibration, we obtained a resolution of 6% for minimum ionization hadrons and 3σ π/K separation for momenta up to 760 MeV/c. Both of these meet the design goals of the BESIII drift chamber. As more data are accumulated at the other resonances in the future, these well-established calibration procedures can be used to continue to achieve accurate ionization measurements and quality particle identification.

References

1 CHAO Kuang-Ta, WANG Yi-Fang. Physics at BES-III. In: Institute of High Energy Physics. International Journal of Modern Physics A, 2009, **24**: 1–21
2 Preliminary Design Report of The BESIII Detector, Jan, 2004
3 WANG Ji-Ke et al. Chin. Phys. C (HEP & NP), 2009, **33**(10): 870–879
4 LIU Jian-Bei. Experimental Study of the BESIII Drift Chamber Performance. 2005 (Ph.D.Thesis) (in Chinese)
5 Blum, Walter, Riegler et al. Particle Detection with Drift Chambers. Berlin Heidelberg: Springer, 2008. 331–359
6 Messel H, Ritson D M. Philos. Mag., 1950, **41**: 1129–1132
7 Telnov A V. BABAR Analysis Document ♯1500, version 4, 2006
8 Todyshev K. BABAR Analysis Document ♯1698, Version 1, 2007
9 Fortin D. BABAR Analysis Document ♯617, Version 1, 2003
10 Dunn J W. Identified Particle Spectra from dE/dx Ionization Measurements in Pb+Pb Collisions at 158 A GeV/c. 1997 (Doctoral thesis)
11 Emi K, Tsukamoto T. Nucl. Instrum. Methods A, 1996, **379**: 225–231
12 Günther J. Particle Identification by dE/dx in the NA35 Time Projection Chamber, IKF-HENPG/8–94
13 Hauschild M. Nucl. Instrum. Methods A, 1996, **379**: 436–441
14 WANG Da-Yong. Track Fitting and dE/dx Offline Software Development and Studies in BESIII. 2006 (Ph. D. Thesis) (in Chinese)
15 Deppe O. Measurment of $D^{*\pm}$ Electroproduction at HERA. 1999 (Doctoral thesis)
16 MA Yuan-Yuan, LIU Jian-Bei et al. High Energy Physics and Nuclear Phyics, 2005, **29**(5):481–484 (in Chinese)
17 Andronic A, Appelshäuser H et al. Nucl. Instrum. Methods A, 2004, **525**: 447–457
18 MA Xiang et al. Chin. Phys. C (HEP & NP), 2008, **32**(9): 744–749